PERGAMON

The International Journal of Biochemistry & Cell Biology 35 (2003) 1548–1557

IJBCB

www.elsevier.com/locate/ijbcb

Structure of the N-terminal extension of human aspartyl-tRNA synthetase: implications for its biological function

Hae-Kap Cheong [a], Jin-Young Park [a], Eun-Hee Kim [a], Chulhyun Lee [a], Sunghoon Kim [b], Youngsoo Kim [c], Byong-Seok Choi [d], Chaejoon Cheong [a,*]

[a] *Magnetic Resonance Team, Korea Basic Science Institute, Daejeon 305-333, South Korea*
[b] *Department of Pharmacy, Seoul National University, Seoul 151-742, South Korea*
[c] *School of Chemical Engineering and Technology, Yeungnam University, Kyongsan 712-749, South Korea*
[d] *Department of Chemistry and National Creative Research Initiative Center, Korea Advanced Institute of Science and Technology, Daejeon 305-701, South Korea*

Received 4 October 2002; received in revised form 4 October 2002; accepted 19 February 2003

Abstract

Human aspartyl-tRNA synthetase (hDRS) contains an extension at the N-terminus, which is involved in the transfer of Asp-tRNA to elongation factor α1 (EF1α). The structure of the N-terminal extension is critical to its function. Conformational studies on the synthetic, 21-residue N-terminal extension peptide (Thr^{5}–Lys^{25}) of human aspartyl-tRNA synthetase using ^{1}H nuclear magnetic resonance (NMR) spectroscopy, showed that the C-terminus adopts a regular α-helix with amphiphilicity, while the N-terminus shows a less-ordered structure with a flexible β-turn. The observed characteristics suggest a structural switch model, such that when the tRNA is in the stretched conformation, the peptide reduces the rate of dissociation of Asp-tRNA from human aspartyl-tRNA synthetase, and provides enough time for elongation factor 1α to interact with the Asp-tRNA. Following Asp-tRNA transfer to EF1α, the peptide assumes the folded conformation. The structural switch model supports the direct transfer mechanism.

Keywords: DRS; NMR structure; Multi-synthetase complex; N-terminal extension

1. Introduction

Protein biosynthesis is a complicated process that requires multiple components. The initial activation of amino acids requires the corresponding aminoacyl-tRNA synthetases (Schimmel & Soll, 1979). The cytoplasmic tRNA synthetases in higher eukaryotes are distinguished from their prokaryotic counterparts by the formation of multi-synthetase complexes. The purified complexes include Asp-, Arg-, Gln-, Ile-, Leu-, Lys-, Met-, and Glu–Pro-tRNA synthetases (Dang & Yang, 1979; Deutscher, 1984; Kellermann et al., 1982; Mirande, 1991). The

Abbreviations: DRS, aspartyl-tRNA synthetase; DQF-COSY, double quantum filtered correlated spectroscopy; EF1α, elongation factor 1α; FID, free induction decay; hDRS, human aspartyl-tRNA synthetase; NMR, nuclear magnetic resonance; NOE, nuclear Overhauser enhancement; NOESY, nuclear Overhauser enhancement spectroscopy; RMD, restrained molecular dynamics; R.M.S.D., root mean square deviation; TFE, 2,2,2-trifluoroethanol; TOCSY, total correlated spectroscopy.

* Corresponding author. Tel.: +82-42-865-3431; fax: +82-42-865-3419.
E-mail address: cheong@kbsi.re.kr (C. Cheong).

1357-2725/03/$ – see front matter © 2003 Elsevier Science Ltd. All rights reserved.
doi:10.1016/S1357-2725(03)00070-0

Asp-tRNA synthetase (DRS) has been cloned from *Escherichia coli* (Eriani, Dirheimer, & Gangloff, 1990), yeast (Sellami, Prevot, Bonnet, Dirheimer, & Gangloff, 1985), rat (Mirande & Waller, 1989), and human (Jacobo-Molina, Peterson, & Yang, 1989; Rho et al., 1999). Extensive sequence similarities have been noted between the DRSs of different species, with the exception of the N-terminal extension of the eukaryotic DRS. Deletions of up to 70 residues of the N-terminal extension of the yeast DRS had no effect on synthetase activity, while deletion of 5 residues at the C-terminus reduced the aminoacylation activity to 80% (Prevost, Eriani, Kern, Dirheimer, & Gangloff, 1989). In the rat and human DRSs, the N-terminal extension was also dispensable for catalytic activity (Agou, Waller, & Mirande, 1996; Escalante & Yang, 1993; Mirande, Lazard, Martinez, & Latreille, 1992).

Nevertheless, accumulating evidence suggests that the synthetase N-terminal extensions play important roles in the structure and function of the multi-tRNA synthetase complex (Jacobo-Molina et al., 1989; Mirande & Waller, 1989; Prevost et al., 1989). Mirande et al. (1992) demonstrated that the in vivo association between the rat DRS and the complex was abolished by the removal of 34 N-terminal residues of DRS. Reed and Yang (1994) suggested that the N-terminal extension played important roles in the release and transfer of Asp-tRNA from the human DRS (hDRS) to elongation factor 1α (EF1α). It was suggested that the N-terminal peptide bound to Asp-tRNA, so that EF1α could join the complex and interact directly with Asp-tRNA, and that the peptide interacted with EF1α to facilitate the release of Asp-tRNA.

Although the proposed functions of the N-terminal extension in DRS seem plausible, it is important to investigate the structural mechanism behind these functions. The secondary structure of the N-terminal extension of the hDRS has been predicted using the Secondary Structure Calculation program (Jacobo-Molina et al., 1989). We report a detailed study of the N-terminal extension peptide (Thr^5–Lys^{256}) of hDRS using nuclear magnetic resonance (NMR) spectroscopy and molecular modeling. On the basis of the obtained structure, we propose a molecular model for the tRNA transfer mechanism that is mediated by structural changes in the N-terminal extension of hDRS.

2. Materials and methods

2.1. Sample preparation

The oligopeptide that constituted the 21 amino acids of the N-terminal extension of hDRS (Table 1) was purchased from Chiron Technologies Ltd. (Melbourne, Australia). 2,2,2-Trifluoroethanol (TFE)-d_3 (99%) and 2,2,3,3-tetradeuterio-3-(trimethylsilyl) propionic acid (TSP) were obtained from Cambridge Isotope Labs (Andover, MA), and sodium phosphate was purchased from Sigma Chemical Co. (St. Louis, MO). The peptide sample for NMR was dissolved in 400 μl of TFE-d_3/50 mM phosphate buffer (pH 7.0) (1:1, v/v) to give a final concentration of about 2 mM.

2.2. NMR spectroscopy

The NMR data were collected using a Bruker DMX600 spectrometer, and processed using XWIN-NMR (Bruker). The proton chemical shifts were referenced to the internal TSP. Two-dimensional spectra were recorded in the phase-sensitive mode using time-proportional phase increments. Solvent suppression was achieved by selective low-power irradiation of the solvent signal during the relaxation delay, or by pulsed field gradients, using the WATERGATE method of Piotto et al. (1992). All of the NMR experiments were performed at 25 °C. The double quantum filtered correlated spectroscopy (DQF-COSY) (Piantini, Sorensen, & Ernst, 1982) spectra were collected as $400(t_1) \times 4096(t_2)$ data points, and the 96 scans made for each free induction decay (FID) were averaged. The data were Fourier-transformed after zero filling to 8192 points in t_2. The final digital resolution was 0.75 Hz per point. The total correlated spectroscopy (TOCSY) (Davis & Bax, 1985) analysis used the MLEV-17 sequence (Bax & Davis, 1985) with a mixing time of 75 ms. The nuclear Overhauser enhancement spectroscopy (NOESY) experiments were carried out with several mixing times (τ_m), within the range of 60–300 ms. The TOCSY and NOESY (Macura, Huang, Suter, & Ernst, 1981) spectra were collected as $512(t_1) \times 2048(t_2)$ data points, and the 64 scans were averaged. After Fourier-transformation, the baselines were corrected using a polynomial function for all the NOESY spectra, prior to measurement of the cross-peak volumes.

Table 1
Proton chemical shift at 298 K of the hDRS N-terminal 21-mer peptide

Residue	NH	αH	βH[a]	γH[a]	Others[a]
Thr[5]	[b]	4.10	3.75	1.26	
Gln[6]	[b]	4.38	1.98, 2.10	2.36	
Arg[7]	8.43	4.29	1.72, 1.81	1.60	δCH_2 3.15, NH 7.29, 6.63
Lys[8]	8.34	4.30	1.73, 1.83	1.41	δCH_2 1.65, εCH_2 2.95
Ser[9]	8.24	4.37	3.89, 3.82		
Gln[10]	8.31	4.32	1.95, 2.11	2.32	
Glu[11]	8.27	4.26	1.90, 2.00	2.23	
Lys[12]	8.13	4.56	1.76	1.43	δCH_2 1.70, εCH_2 2.94
Pro[13]		4.36	1.89, 2.33	1.98, 2.03	δCH_2 3.54, 3.76
Arg[14]	8.21	4.13	1.80	1.66	δCH_2 3.16, NH 6.63, 7.32
Glu[15]	8.74	4.18	1.95	2.03, 2.27	
Ile[16]	7.89	4.02	1.87	1.16, 1.43	γCH_3 0.86, δCH_3 0.80
Met[17]	7.94	4.31	2.07	2.46, 2.56	εCH_3 2.00
Asp[18]	8.16	4.52	2.66		
Ala[19]	7.89	4.23	1.40		
Ala[20]	8.06	4.16	1.39		
Glu[21]	8.05	4.12	1.91, 1.97	2.23	
Asp[22]	8.01	4.50		2.55	
Tyr[23]	7.76	4.45	2.94, 3.07		2,6H 7.08, 3,5H 6.77
Ala[24]	7.83	4.28	1.32		
Lys[25]	7.48	4.11	1.79	1.37	δCH_2 1.65, εCH_2 2.95

[a] Stereo-specific assignments were not made.
[b] Could not be assigned by terminal flexibility.

2.3. Structure calculation

We obtained 165 distance restraints for the structural calculations from the NOESY spectra, with mixing times of 60, 150, and 300 ms. The cross-peak intensities were converted into four upper bounds of the distance restraints, i.e. 2.5, 3.2, 4.0, and 5.0 Å. In all cases, the lower bounds were defined as the sum of the van der Waals radii (1.8 Å) of the interacting protons. The 9 $^3J_{HN\alpha}$ values (4–6 Hz for residues 15–24) were converted into loose dihedral angle restraints of $-100^\circ < \Phi < -20^\circ$. A force constant of 15 kcal/mol was used to enforce the restraints. Hydrogen-bonding restraints were not used. The structure of the 21-residue N-terminal extension of hDRS was calculated using DG II and DISCOVER (Molecular Simulations Inc., San Diego, CA), together with INSIGHT II as the graphic interface. The AMBER force field was used for structure refinement. Triangle inequality bound smoothing and four-dimensional embedding procedures were used for the distance geometry calculation using DG II. The generated structures were then refined by simulated annealing at 2000 K for 6000 ps with a step size of 0.3 ps, followed by 400 steps of conjugate gradient energy minimization. From the 50 trials, we selected 21 structures that had distance violations <0.3 Å and dihedral angle violations of $<2^\circ$. These structures were refined further by restrained energy minimization and dynamics. The distance-dependent dielectric constant was used. The structures were first minimized until the change in energy was less than 0.001 kcal/Å, using the steepest descent and conjugate gradient methods. After minimization, the structures were subjected to molecular dynamics for 100 ps at 300 K. The structures were allowed to equilibrate over the first 40 ps of the restrained molecular dynamics (RMD) runs, and then averaged over the final 60 ps. The averaged structures were minimized for subsequent analyses of potential energies and convergence.

2.4. Surface plasmon resonance analysis

The binding affinity of the hDRS N-terminal extension for tRNA-Asp was determined by surface plasmon resonance, using a BIAcore^{TM}2000 biosensor

system and BIA evaluation software (version 3.0; BIAcore AB, Uppsala, Sweden). The peptide was immobilized on research-grade CM5 sensor chips, at a concentration of 1 mg/ml in 10 mM HEPES (pH 7.4), 150 mM NaCl, 3.4 mM EDTA, and 0.005% (v/v) surfactant P_{20}, using the amine coupling kit that was supplied by the manufacturer. Approximately 100 RU of the peptide was immobilized under these conditions, where 1000 RU corresponds to an immobilized protein concentration of 1 ng/mm^2. Calf liver tRNA was from Biogenics. Five binding cycles using different tRNA concentrations were performed with a constant flow (10 μl/min) of a buffer that contained 20 mM Tris–HCl (pH 6.5), 250 mM NaCl, 1 mM $MgCl_2$, 1 mM DTT, and 0.1 mM EDTA. Once the injected tRNA passed the surface, the formed complexes were washed with the buffer for 9 min. Non-specific binding of tRNA to the carboxymethylated dextran-coated sensor chip was subtracted to obtain corrected sensorgrams. All of the experiments were performed at 25 °C. The data were collected at 1 Hz, and analyzed on the assumption of first-order binding kinetics.

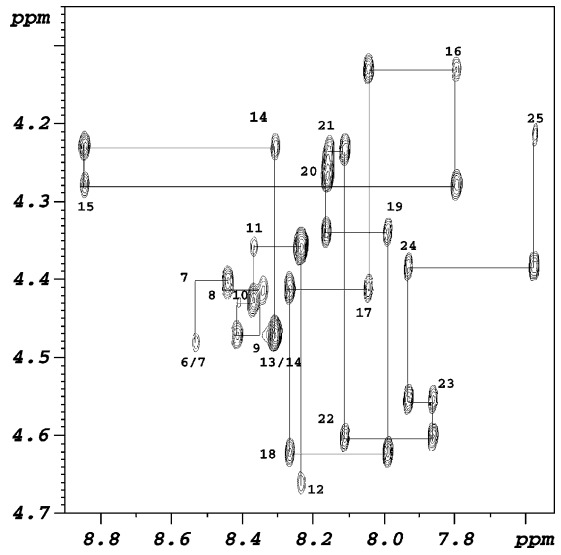

Fig. 1. Expanded H_α(D2)–H_N(D1) region of the NOESY spectrum (300 ms mixing time) for the hDRS N-terminal 21-mer peptide in TFE/H_2O. The spectrum was recorded at 298 K. The $d_{\alpha N}$ sequential connectivity is shown.

3. Results

3.1. Secondary structure determination

The DQF-COSY and TOCSY spectra were used to assign individual spin systems for each amino acid, which were then sequentially assigned to key NOESY cross-peaks in the fingerprint region (Fig. 1), using the standard method (Wüthrich, 1986). The chemical shifts are listed in Table 1.

The chemical shift differences of $C_\alpha H$ and NH between the random coil (Wüthrich, 1986) and the N-terminal peptide are shown in Fig. 2a. The upfield shifts of the α-protons in the C-terminal part of the peptide were compatible with a helical structure. The chemical shift index (CSI) (Wishart, Sykes, & Richards, 1992) of $C_\alpha H$ showed a stretch of −1, from residues Arg^{14} through Tyr^{23} (Fig. 2b), which also signifies a helical structure. The sequential and medium range nuclear Overhauser enhancement (NOE) connectivities in the NOESY spectra, and the $^3J_{HN\alpha}$ values from the NH-$C_\alpha H$ cross-peaks in the DQF-COSY spectra were analyzed (Fig. 3), and showed a good correlation with the chemical shift

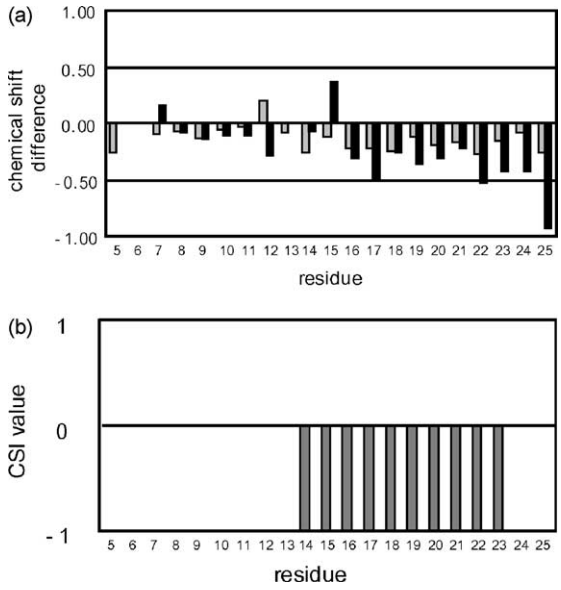

Fig. 2. (a) Plot of the chemical shift differences between the observed values of H_α and H_N and the corresponding random coil values. (b) CSI value of H_α.

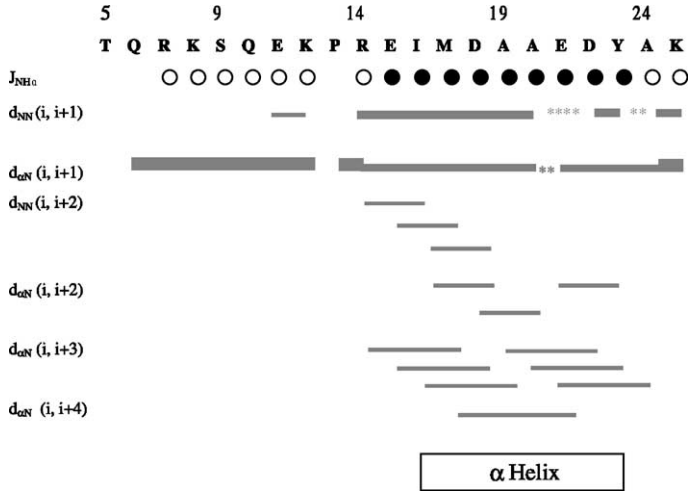

Fig. 3. Amino acid sequence of the hDRS N-terminal peptide, and a summary of the sequential and medium-range NOEs; the spin-spin coupling constants are indicated as follows: (○), 7–9 Hz; (●), 4–6 Hz. The thick and thin bars represent the strong and weak NOE intensities, respectively. The lines that start and end at the positions of the interacting residues indicate NOE connectivity. (∗∗), overlapping NOE cross-peaks.

index of $C_\alpha H$ (Fig. 2b). Indeed, a number of the NOE connectivities, i.e. d_{NN} (i, $i+1$), d_{NN} (i, $i+2$), $d_{\alpha N}$ (i, $i+2$), and $d_{\alpha N}$ (i, $i+3$), and the low values of $^3J_{HN\alpha}$ (4–6 Hz) from Glu^{15} to Tyr^{23} strongly suggest the existence of a significant population of conformers that contain a well defined α-helix in that part of the peptide. In the N-terminal part of the peptide, the $^3J_{HN\alpha}$ values, which ranged from 7 to 9 Hz, together with the intense $C_\alpha H$-NH (i, $i+1$) NOEs, and the lack of medium-range NOEs, suggest the presence of conformational fluctuations.

3.2. Conformation of the peptide

Unambiguous assignments and restraints were derived from the NOEs and $^3J_{HN\alpha}$ values, which permitted the generation of structures that were consistent with the experimental data. The peptide consisted of the flexible N-terminal region, a β-turn, and an amphiphilic helix in the C-terminal region. We obtained 21 final structures (Fig. 4B) with backbone root mean square deviation (R.M.S.D.) values of 0.55 ± 0.26 Å for the well-defined helical region (residues 16–23) and 0.88 ± 0.35 Å for the β-turn region (residues 11–14). The statistics of the final structures and the hydrogen bonds that were observed in the converged helical region are listed in Table 2. The Ramanchandran plot statistics were analysed by PROCHECK version 3.5.4 (Laskowski, MacArthur, Moss, & Thornton, 1993). The Asp^{18} carbonyl oxygen formed a bifurcated hydrogen bond with the amide protons of both Glu^{21} and Asp^{22}. The expected hydrogen bond between Met^{17} and Glu^{21} was not observed. This conformation lessens the electrostatic repulsion between Asp^{18} and Asp^{22}, and allows Glu^{21} to slide into the hydrophilic side of the amphiphilic helix. The terminal (i, $i+3$) hydrogen bond between Glu^{21} and Ala^{24}, which has a 3_{10}-helix character and sometimes appears at the end of the α-helix, was also observed.

Examination of the side-chain orientations revealed that the helix was amphiphilic, with the hydrophobic residues on one side of the helix and the hydrophilic residues on the opposite side. Representative structures that illustrate the amphiphilic characteristics of the well-defined helical region are shown in Fig. 4A. It was suggested previously (Jacobo-Molina et al., 1989) that the secondary structure of the DRS N-terminal extension consisted of a neutral amphiphilic helix, and it was assumed that the helical structure was present throughout the whole peptide, and that the hydrophilic side was neutral,

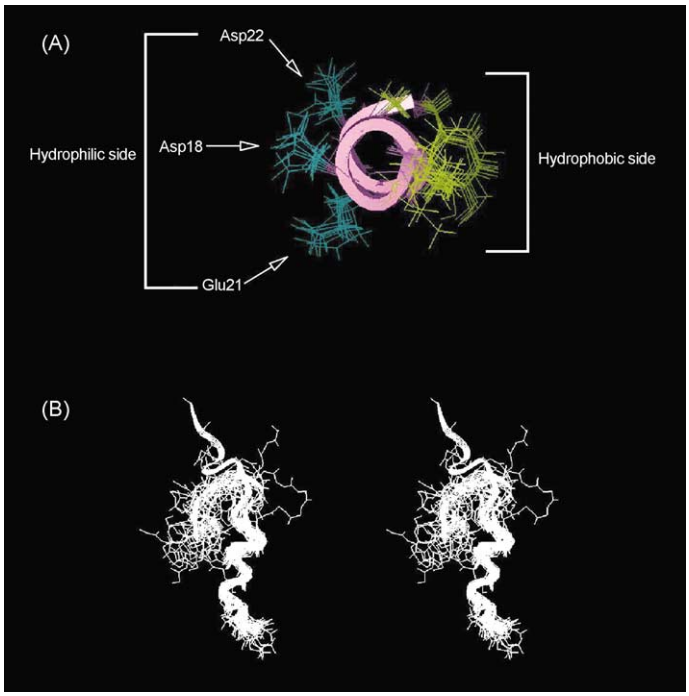

Fig. 4. (A) Helical region of the peptide, viewed down the long axis, with the hydrophobic residues in yellow and the hydrophilic residues in blue. (B) Stereoview of all the backbone atoms (N-terminus on top) superimposed over the heavy atoms, from residues Ile^{16} to Tyr^{23} of the final 21 structures.

since it had both positively and negatively charged residues. Our results show that the positively charged residues are not involved in the helical structure, and that only the negatively charged Asp^{18}, Glu^{21}, and Asp^{22} residues face one side of the helix, while the opposite side is composed of hydrophobic residues. Analysis of the conformation of the N-terminal part of the peptide revealed that this region had a type IV β-turn (from Glu^{11} to Arg^{14} for some conformers, and from Gln^{10} to Pro^{13} for the others). The type IV β-turn is less rigid than the other types of β-turn. This type IV β-turn loosely restricts the range of the conformational spread in the N-terminal part of the peptide.

Some of the structures defined here show that the two positively charged residues (Arg^7 and Lys^8) at the N-terminus come in close contact with the negatively charged residues (Asp^{18}, Glu^{21}, and Asp^{22}) on the hydrophilic side of the helix (Fig. 5). This favorable interaction is made possible by the formation of the β-turn.

3.3. Direct interaction between the peptide and tRNA

The feasibility of a direct interaction between the N-terminal extension and tRNA was tested using surface plasmon resonance analysis. The sensorgram (Fig. 6) shows that the immobilized peptide interacts with Asp-tRNA, although the binding may not be site-specific, since the dissociation constant was calculated to be 3.8 ± 0.2 μM.

4. Discussion

Although TFE is known to promote helix structure, recent studies have shown that not all peptides assume the helical conformation in the presence of TFE (Dyson, Merutka, Waltho, Lerner, & Wright, 1992; Dyson, Sayre, et al., 1992). Thus, it appears that TFE acts only within the context of a pre-existing helix-coil equilibrium (Jasanoff & Fersht, 1994), rather than

Table 2
Structure determination statistics

	R.M.S.D.		Hydrogen bonds	
	Backbone	Heavy atoms	Donor NH	Acceptor CO
Helix part (16–23)	0.55 ± 0.26	1.54 ± 0.39		
β-Turn (11–14)	0.88 ± 0.35	2.50 ± 0.97		
			Asp^{18}	Arg^{14}
			Ala^{19}	Glu^{15}
			Ala^{20}	Ile^{16}
			Glu^{21}	Asp^{18}
			Asp^{22}	Asp^{18}
			Tyr^{23}	Ala^{19}
			Ala^{24}	Glu^{21}
Number of NOE distance restraints				
Intra	24			
Sequential	72			
Medium	69			
Energy analysis				
Total energy	−467.5 ± 26.2			
Bond energy	6.5 ± 0.6			
Theta energy	46.7 ± 4.3			
Phi energy	54.1 ± 7.1			
Out-of-plane energy	5.7 ± 1.4			
Hydrogen bond energy	8.9 ± 1.9			
Non-bond energy	−18.0 ± 6.3			
Coulomb energy	−553.6 ± 24.7			
Forcing potential	−17.4 ± 4.0			
Ramanchandran plot statistics (%)				
Residues in allowed regions	97.9			
Most favored regions	53.2			
Additionally allowed regions	37.0			
Generously allowed regions	7.7			
Residues in disallowed regions	2.1			

All of the energy values are given in kcal/mol, and the distances are given in Å.

creating the helical structure itself. In the absence of TFE, we were unable to observe any secondary structures or stable conformations in the CD and NMR spectra, which suggests that this peptide does not exist as a single conformation, even in 50% TFE. The $J_{HN\alpha}$ values (Fig. 3) represent the averaged values of the conformational ensembles. Therefore, the structure presented here should be regarded as one of the highly populated conformational states of the hDRS N-terminal extension in solution. Thus, we assume that the N-terminal extension has helical properties at the protein level, and that 50% TFE may mimic the environment of the extension in the whole protein.

Elucidation of the structure of the N-terminal extension in the context of the whole enzyme is critical to understanding its function. Unfortunately, the solution and crystal structures of aminoacyl-tRNA synthetases that contain the extension have not been reported to date. Based on their chromatographic studies, Reed and Yang (1994) suggested that the N-terminal peptide in hDRS could bind to tRNA and EF1α. Our surface plasmon resonance experiments support the idea of a direct interaction between the N-terminal peptide and tRNA. The molecular model of the crystal structure of the yeast Asp-tRNA–DRS complex places the N-terminal extension within interacting distance of the tRNA. The N-terminal extension can have two distinct conformations, as shown in Fig. 5. From the above results, we propose a structural switch model. When tRNA is bound, the positively charged residues of the

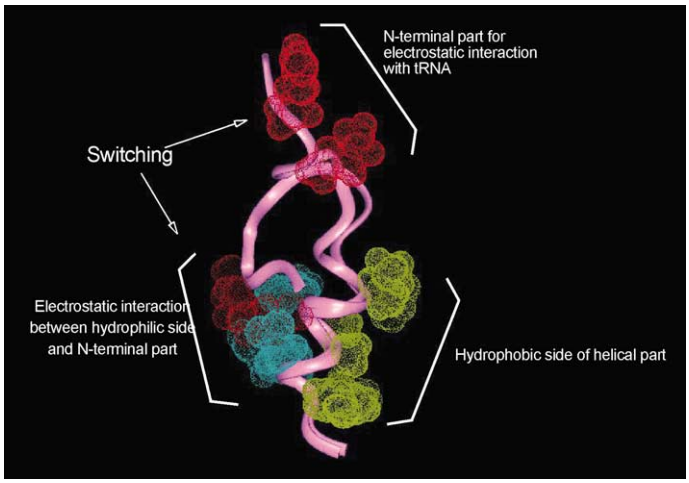

Fig. 5. The structural switch model of the N-terminal extension peptide. Two representative structures (from the 21 final structures) are shown, with the backbone ribbons in pink, the side-chain surfaces (Ile^{16}, Ala^{19}, Ala^{20}, and Tyr^{23}) on the hydrophobic side of the helical region in yellow, the side-chain surfaces (Asp^{18}, Glu^{21}, and Asp^{22}; negatively charged residues) on the hydrophilic side of helical region in blue, and the side-chain surfaces (Arg^{7} and Lys^{8}; positively charged residues) on the flexible part of the N-terminal region in red. The positively charged residues in the flexible N-terminal region supposedly play a switching role in the function of hDRS.

flexible N-terminal part of the peptide interact with the tRNA. The N-terminal extension holds Asp-tRNA and reduces the rate of dissociation of Asp-tRNA from the hDRS. When the tRNA is transferred to EF1α, the N-terminal part folds back, and interacts with the negatively charged residues of the helix, thereby facilitating the release of Asp-tRNA. This model should be regarded as a tentative one, since the entire

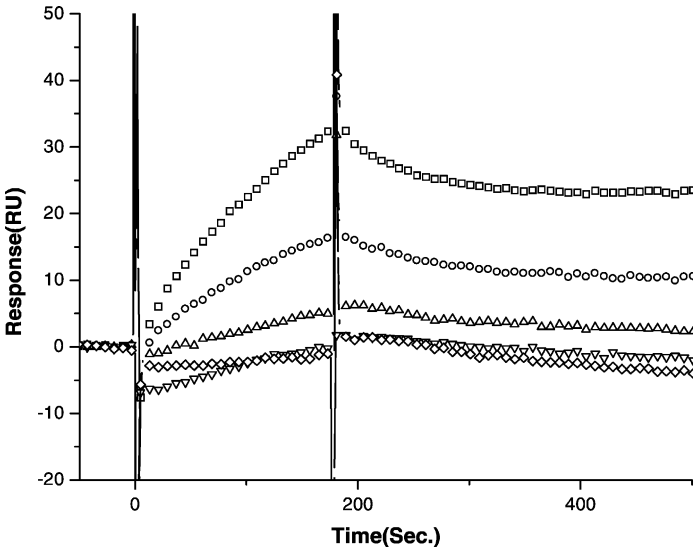

Fig. 6. Surface plasmon resonance sensorgram. The overlaid sensorgrams of tRNA that was injected over the surface with 100 RU of immobilized hDRS N-terminal extension peptide. The tRNA was solubilized in buffer (see *Materials and Methods* section) at concentrations of 23 μM (□), 11.5 μM (○), 5.7 μM (△), 2.8 μM (▽), and 1.4 μM (◇).

structure of the tRNA-synthetase complex has not yet been solved.

The biological importance of the hDRS N-terminal extension has been suggested to lie in the enhancement of the direct transfer of Asp-tRNA to EF1α (Reed, Wastney, & Yang, 1994; Reed & Yang, 1994). Kinetic studies on the mechanism of transfer of Asp-tRNA from hDRS to EF1α have shown that Asp-tRNA is transferred directly to EF1α (Reed et al., 1994). The deletion and kinetic studies have further suggested that the N-terminal extension enhances the direct transfer of Asp-tRNA to EF1α by reducing the rate of dissociation of Asp-tRNA from hDRS (Reed & Yang, 1994). The structural switch model derived from our results supports this direct transfer mechanism.

In our proposed structure for the peptide, the hydrophobic face of the helical portion is probably involved in the protein–protein interaction. As mentioned above, the interaction of the extension motif with EF1α facilitates the release of the Asp-tRNA. The results of preliminary experiments by Reed and Yang (1994) suggest that the C-terminal half of the extension motif of hDRS may be essential for the interaction with EF1α. The protein–protein interaction between the hydrophobic side of the helical portion and EF1α may induce structural changes in the Asp-tRNA–hDRS complex, thereby facilitating the release of Asp-tRNA. In addition, this release may be mediated by the repulsion of the negatively charged hydrophilic side by the Asp-tRNA.

The activity of the yeast DRS differs slightly from that of the hDRS (this study). The N-terminal extension of yeast DRS forms a fully induced helix with 23 amino acid residues (Agou, Yang, Gequière, Waller, & Guittet, 1995). The helix shows amphiphilic character, although the hydrophilic side is composed of positively charged residues. This basic amphiphilic helix may be induced by polyanion. Cationic residues segregate to one side of the helical structure, thus providing an ideal polycationic interface for binding to polyanionic surfaces. Agou et al. (1995) proposed that this structural motif might participate in non-specific tRNA–protein interactions. Therefore, their model does not involve structural switching of the N-terminal extension.

Acknowledgements

This work was supported by the National Research Laboratory Program and Strategic National R&D Program (to C.C.), and supported in part by the National Creative Research Initiatives Program (to B.-S.C.) of the Ministry of Science and Technology, the Republic of Korea.

References

Agou, F., Waller, J. P., & Mirande, M. (1996). Expression of rat aspartyl-tRNA synthetase in Saccharomyces cerevisiae. Role of the NH2-terminal polypeptide extension on enzyme activity and stability. *The Journal of Biological Chemistry*, *271*, 29295–29303.

Agou, F., Yang, Y., Gequière, J. C., Waller, J. P., & Guittet, E. (1995). Polyanion-induced alpha-helical structure of a synthetic 23-residue peptide representing the lysine-rich segment of the N-terminal extension of yeast cytoplasmic aspartyl-tRNA synthetase. *Biochemistry*, *34*, 569–579.

Bax, A., & Davis, D. G. (1985). MLEV-17-based two-dimensional homonuclear magnetization transfer spectroscopy. *Journal of Magnetic Resonance*, *65*, 355–360.

Dang, C. V., & Yang, D. C. H. (1979). Disassembly and gross structure of particulate aminoacyl-tRNA synthetases from rat liver. Isolation and the structural relationship of synthetase complexes. *The Journal of Biological Chemistry*, *254*, 5350–5356.

Davis, D. G., & Bax, A. (1985). Assignment of complex proton NMR spectra via two-dimensional homonuclear Hartmann–Hahn spectroscopy. *Journal of American Chemical Society*, *107*, 2820–2823.

Deutscher, M. P. (1984). The eucaryotic aminoacyl-tRNA synthetase complex: Suggestions for its structure and function. *Journal of Cell Biology*, *99*, 373–377.

Dyson, H. J., Merutka, G., Waltho, J. P., Lerner, R. A., & Wright, P. E. (1992). Folding of peptide fragments comprising the complete sequence of proteins. Models for initiation of protein folding. I. Myohemerythrin. *Journal of Molecular Biology*, *226*, 795–817.

Dyson, H. J., Sayre, J. R., Merutka, G., Shin, H. C., Lerner, R. A., & Wright, P. E. (1992). Folding of peptide fragments comprising the complete sequence of proteins. Models for initiation of protein folding. II. Plastocyanin. *Journal of Molecular Biology*, *226*, 819–835.

Eriani, G., Dirheimer, G., & Gangloff, J. (1990). Aspartyl-tRNA synthetase from *Escherichia coli*: Cloning and characterisation of the gene. *Nucleic Acid Research*, *18*, 7109–7117.

Escalante, C., & Yang, D. C. H. (1993). Expression of human aspartyl-tRNA synthetase in *Escherichia coli*. Functional analysis of the N-terminal putative amphiphilic helix. *The Journal of Biological Chemistry*, *268*, 6014–6023.

Jacobo-Molina, A., Peterson, R., & Yang, D. C. H. (1989). cDNA sequence, predicted primary structure, and evolving amphiphilic

helix of human aspartyl-tRNA synthetase. *The Journal of Biological Chemistry*, *264*, 16608–16612.

Jasanoff, A., & Fersht, A. R. (1994). Quantitative determination of helical propensities from trifluoroethanol titration curves. *Biochemistry*, *33*, 2129–2135.

Kellermann, O., Tonnetti, H., Brevet, A., Mirande, M., Paillez, J. P., & Waller, J. P. (1982). Macromolecular complexes from sheep and rabbit containing seven aminoacyl-tRNA synthetases. I. Species specificity of the polypeptide composition. *The Journal of Biological Chemistry*, *257*, 11041–11048.

Laskowski, R. A., MacArthur, M. W., Moss, D. S., & Thornton, J. M. (1993). PROCHECK: A program to check the stereochemical quality of protein structures. *Journal of Applied Crystallography*, *26*, 283–291.

Macura, S., Huang, Y., Suter, D., & Ernst, R. R. (1981). Two-dimensional chemical exchange and cross-relaxation spectroscopy of coupled nuclear spins. *Journal of Magnetic Resonance*, *43*, 259–281.

Mirande, M. (1991). Aminoacyl-tRNA synthetase family from prokaryotes and eukaryotes: Structural domains and their implications. *Progress in Nucleic Acid Research and Molecular Biology*, *40*, 95–142.

Mirande, M., Lazard, M., Martinez, R., & Latreille, M. T. (1992). Engineering mammalian aspartyl-tRNA synthetase to probe structural features mediating its association with the multisynthetase complex. *European Journal of Biochemistry*, *203*, 459–466.

Mirande, M., & Waller, J. P. (1989). Molecular cloning and primary structure of cDNA encoding the catalytic domain of rat liver aspartyl-tRNA synthetase. *The Journal of Biological Chemistry*, *264*, 842–847.

Piantini, U., Sorensen, O. W., & Ernst, R. R. (1982). Multiple quantum filters for elucidating NMR coupling networks. *Journal of American Chemical Society*, *104*, 6800–6801.

Piotto, M., Saudek, V., & Sklenar, V. (1992). Gradient-tailored excitation for single-quantum NMR spectroscopy of aqueous solutions. *Journal of Biomolecular NMR*, *2*, 661–665.

Prevost, G., Eriani, G., Kern, D., Dirheimer, G., & Gangloff, J. (1989). Study of the arrangement of the functional domains along the yeast cytoplasmic aspartyl-tRNA synthetase. *European Journal of Biochemistry*, *180*, 351–358.

Reed, V. S., Wastney, M. E., & Yang, D. C. H. (1994). Mechanisms of the transfer of aminoacyl-tRNA from aminoacyl-tRNA synthetase to the elongation factor 1 alpha. *The Journal of Biological Chemistry*, *269*, 32932–32936.

Reed, V. S., & Yang, D. C. H. (1994). Characterization of a novel N-terminal peptide in human aspartyl-tRNA synthetase. Roles in the transfer of aminoacyl-tRNA from aminoacyl-tRNA synthetase to the elongation factor 1 alpha. *The Journal of Biological Chemistry*, *269*, 32937–32941.

Rho, S. B., Kim, M. J., Lee, J. S., Seol, W., Motegi, H., Kim, S., & Shiba, K. (1999). Genetic dissection of protein–protein interactions in multi-tRNA synthetase complex. *Proceedings of the National Academy of Sciences of the United States of America*, *96*, 4488–4493.

Schimmel, P., & Soll, D. (1979). Aminoacyl-tRNA synthetases: General features and recognition of transfer RNAs. *Annual Reviews of Biochemistry*, *48*, 601–648.

Sellami, M., Prevot, G., Bonnet, J., Dirheimer, G., & Gangloff, J. (1985). Isolation and characterization of the yeast aspartyl-tRNA synthetase gene. *Gene (Amsterdam)*, *40*, 349–352.

Wishart, D. S., Sykes, B. D., & Richards, F. M. (1992). The chemical shift index: A fast and simple method for the assignment of protein secondary structure through NMR spectroscopy. *Biochemistry*, *31*, 1647–1651.

Wüthrich, K. (1986). *NMR of protein and nucleic acids*. New York: Wiley/Interscience.